Comparative Analysis of Binding Energy of Chymostatin with Human Cathepsin A and Its Homologous Proteins by Molecular Orbital Calculation

Tatsusada Yoshida,[†] Zsolt Lepp,[†] Yoshito Kadota,[†] Yurie Satoh,[†] Kohji Itoh,[†,‡] and Hiroshi Chuman*[,†]

Institute of Health Biosciences, The University of Tokushima Graduate School, 1-78 Shomachi, Tokushima 770-8505, Japan, and CREST, JST, 4-1-8 Honcho, Kawaguchi, Saitama 332-0012, Japan

Received March 16, 2006

Cathepsin A is a mammalian lysosomal enzyme that catalyzes the hydrolysis of the carboxy-terminal amino acids of polypeptides and also regulates β-galactosidase and neuraminidase-1 activities through the formation of a multienzymic complex in lysosomes. Human cathepsin A (hCathA), yeast carboxypeptidase (CPY), and wheat carboxypeptidase II (CPW) belong to the α/β-hydrolase fold family. They have structurally similar active-site clefts, but there are small differences in the amino acid residues comprising their active sites that might determine the substrate specificity and sensitivity to microbial inhibitors including chymostatin. To examine the selectivity and binding mechanism of chymostatin as to hCathA, CPY, and CPW at the atomic level, we analyzed the interaction energy between chymostatin and each protein quantitatively by semiempirical molecular orbital calculation AM1 with the continuum solvent model. We predicted the electrostatic repulsion between the P3 cyclic arginine residue of the inhibitor and the Arg344 in the S3 active substite of hCathA. Genetic conversion of Arg344 of the wild-type hCathA to Ile also caused an increase in its sensitivity to chymostatin, which was correlated with the decrease in the interaction energy calculated with the molecular orbital method. The present results suggest that such molecular calculation should be useful for evaluating the interactions between ligands, including inhibitors and homologous enzymes, in their docking models.

INTRODUCTION

Human cathepsin A (hCathA; EC3.4.16.1) is a serine exopeptidase that exhibits carboxypeptidase activity at acidic pH and deamidase/esterase activities at neutral pH toward artificial substrates and a set of bioactive peptides including tachykinins and endothelin-1.[1−3] CathA is also identical to a lysosomal protective protein (PPCA) that has a protective function as to lysosomal glycosidases including β-galactosidase (β-Gal; EC3.2.1.23) and neuraminidase-1 (NEU1; EC3.2.1.18) through the formation of a multimeric complex in lysosomes to protect β-Gal from proteolytic degradation and to activate NEU1.[4−6] This specific glycoprotein is synthesized as a catalytically inactive precursor/zymogen and proteolytically processed to the active mature two-chain (32/20 kDa) form.[3,5,6] The mature form is also secreted from human platelets and lymphoid cells,[1,7] suggesting an extracellular function of CathA's.

Galactosialidosis is an autosomal recessive inherited metabolic disease caused by a genetic defect of PPCA, associated with the simultaneous loss of β-Gal and NEU1 as well as CathA and deamidase activities, and excessive accumulation of their natural substrates. A variety of clinical symptoms develop, including cerebellar ataxia, myoclonus, cherry-red spots, angiokeratoma, skeletal dysplasia, hepatosplenomegaly, and so forth.[4,7] The relationship between the excessive accumulation of glycoconjugates and the clinical manifestations has been discussed.[4] However, the pathophysiological significance of CathA deficiency has not been established, although an abnormal distribution of endothelin-1 as a possible natural substrate was demonstrated in brains from patients.[8] Therefore, it would be useful to develop a specific inhibitor of hCathA as a tool for analysis of its pathophysiological roles.

Serine carboxypeptidases comprise a group of exopeptidases that catalyze the hydrolysis of the carboxyl terminal amino acids of peptides and proteins, have a Ser-His-Asp "catalytic triad" in their active-site clefts, and are inactivated by specific serine protease inhibitors including diisopropyl fluorophosphates. They are classified into two types: C-type carboxypeptidases (EC3.4.16.5), with a preference for a hydrophobic amino acid residue at the P1′ position, and D-type carboxypeptidases (EC3.4.16.6), with a high affinity for positively charged (basic) P1′ residues.[9] Yeast carboxypeptidase Y (CPY) and wheat serine carboxypeptidase II (CPW) are typical C-type and D-type enzymes, respectively.[10,11] On the other hand, CathA preferentially catalyzes the hydrolysis of N-blocked dipeptides having aromatic and large hydrophobic amino acids at the P1 and P1′ positions as well as positively charged residues at the P1′ position at acidic pH.[12] The hCathA precursor dimer was demonstrated to exhibit structural similarity to CPY and CPW on the basis of their X-ray crystal structures,[13] although they exhibit only about 30% overall primary sequence identity. All of these enzymes have the conserved Ser-Asp-His catalytic triad (hCathA, Ser150-Asp372-His429; CPW, Ser146-Asp338-

* Corresponding author tel.: +81-88-633-7257; fax: +81-88-633-9508; e-mail: hchuman@ph.tokushima-u.ac.jp.
[†] The University of Tokushima Graduate School.
[‡] CREST.

10.1021/ci060093p CCC: $33.50
Published on Web 09/06/2006

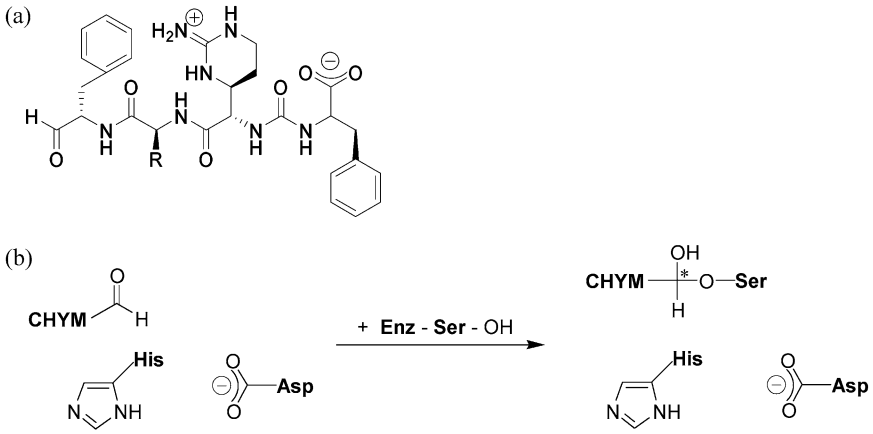

Figure 1. (a) Structure of chymostatin. Chymostatin is isolated as a mixture of three forms; R takes Leu, Val, and Ile. The R group is Leu in the X-ray structure of the complex of CPW with chymostatin. (b) Possible mechanism of forming the tetrahedral intermediate between chymostatin (CHYM) and the active Ser residue in the catalytic triad. The intermediate has an asymmetric carbon atom (*).

His397; CPY, Ser146-Asp338-His397) and oxyanion hole (hCathA, Gly57-Tyr151; CPW, Gly53-Tyr147; CPY, Gly53-Tyr147) in their active-site clefts and belong to the so-called α-/β-hydrolase fold family.[10−15]

Chymostatin, *N*-[(*S*)-1-carboxy-isopentyl]-carbamoyl-α-(2-iminohexahydro-4(*S*)-pyrimidyl)-L-glycyl-L-phenylalaninal (Figure 1a),[16] was reported to be a potent inhibitor of CPW.[17] We also have analyzed comparatively the effects of microbial serine carboxypeptidase inhibitors, including chymostatin, on homologous hCathA, CPW, and CPY and demonstrated their different sensitivities to each inhibitor.[18] The chemical reaction between the aldehyde group of chymostatin and Ser-OH takes place, and then, it gives the tetrahedral intermediate as shown in Figure 1b. This intermediate is considered to be the final product of this reaction. The experimental free energetic difference (ΔG^{exp}) in the above process is small, and hence, the reaction barrier height of this process is considered to be low and to be nearly linear to ΔG^{exp} between the initial and final systems.

Quantum chemical calculations of large molecular systems such as proteins have been considered to be useful for understanding the detailed mechanism of their related phenomena at the electronic level. In fact, a quantum mechanical approach was shown to be powerful in the study of chemical reactions in solution[19] and in a protein.[20] It had been desired to develop practical methods to calculate a large biomolecular system quantum mechanically. For many years, a number of methods employing the combination of quantum mechanics with classical molecular mechanics (QM/MM) have been developed. Warshel and Levit,[21] the pioneers of QM/MM, demonstrated this approach to be quite useful for the study of enzymatic reactions in solution. Recently, an advanced QM/MM approach was shown to be a most powerful tool for investigating an enzymatic mechanism.[22] However, a major problem of this approach has been pointed out to be the treatment of the QM/MM boundary in systems where covalent bonds are formed and broken. To avoid this problem, Merz et al.[23] proposed a combined quantum mechanical/quantum mechanical (QM/QM) method, which was applicable to a large system. Recently, as a result of progress in computational algorithms and machine power, efficient molecular orbital methods for calculating a full biomolecular system have been developed. They are the variational linear scaling method LocalSCF[24] at the semiempirical AM1 level of theory and the ab initio fragment molecular orbital (FMO) method.[25−27] These methods are free from the above problem and enable the calculations of proteins consisting of ∼500 amino acid residues very efficiently.

In this work, we used the LocalSCF and molecular dynamics (MD) calculation to elucidate the chymostatin-binding mechanism and to reveal the structural factors that govern the binding selectivity for each enzyme in comparison with experimental results.

MATERIALS AND METHODS

Materials. Chymostatin was purchased from the Peptide Institute (Osaka, Japan). CPY, *N*-benzyloxycarbonyl-L-phenylalanyl-L-leucine (Z-Phe-Leu), fetal calf serum (FCS), and Ham's F-10 were from Sigma (St. Louis, MO). CPW was from Wako Pure Chemicals (Osaka, Japan). Geneticin (G418) was from GIBCO/BRL (Grand Island, NY). The reagents and enzymes for molecular biology were from Nippon Gene (Osaka, Japan) and Takara (Tokyo, Japan).

Construction of an Expression Vector for Mutant PPCA(Arg344Ile). pCXPPCA plasmid DNA[7] was used as a template for polymerase chain reaction with the following primers to introduce the base substitutions (1120C → A and 1121G → T) causing the corresponding amino acid substitution (Arg344 to Ile) in the wild-type human PPCA cDNA and to create a SmaI−SacI restriction site at the 5′ and 3′ ends, respectively: forward, 5′-CTTACAGTACCGCATTCTCTACCGAAGCAT-3′; reverse, 5′-ATGCTTCGGTAGAGAATGCGGTACTGTAAG-3′. The amplified cDNA fragment was subcloned into the SmaI−SacI site of pCXPPCA, generating pCXPPCA(R344I).

Cell Culture and Establishment of a Fibroblastic Cell Line Stably Expressing Mutant PPCA(R344I). A fibroblastic cell line, ASVGS-1, derived from a galactosialidosis patient[7] and a transformed ASVGS-1 cell line expressing the wild-type PPCA cDNA (T1-PPCA)[18] were maintained in Ham's F-10 medium supplemented with 10% (v/v) FCS at 37 °C in the presence of 5% CO_2.

ASVGS-1 cells (1×10^5) were seeded on 60-mm dishes on the day before the addition of pCXPPCA(R344I) plasmid DNA. Lipofection of 10 μg of pCXPPCA(R344I) with cationic lipid reagent Unifector (B-bridge International Inc., San Jose, CA) was performed. A total of 24 h after

transfection, the cells were washed with phosphate-buffered saline and then cultured in fresh Ham's F-10 medium containing 10% FCS. After 2 days, the cells were trypsinized and split 1:5 into 100-mm dishes, and then, G418-resistant cell lines were selected containing Ham's F-10 with 10% FCS and a final 800 μg/mL of G418 and designated as T1-PPCA(R344I).

Enzyme Assays and Protein Determination. CathA activity was measured with Z-Phe-Leu as the substrate at optimal pH 5.6.[18] The K_i values were measured as described previously.[28] Protein determination was performed with a D*C* protein assay kit (Bio-Rad, Hercules, CA) and bovine serum albumin as the standard.

Inhibition Study on Human CathA, its R344I Mutant, CPW, and CPY. As the source of the wild-type hCathA and its R344I mutant, cell extracts of the T1-PPCA and T1-PPCA(R344I) cell lines were used, respectively. A total of 1×10^7 cells of each were homogenized by sonication in nine volumes of pure water, followed by centrifugation at 15 000*g* for 15 min. The resultant supernatant was used as the cell extract.

The inhibition assay was performed under two different pH's in 50 mM sodium acetate buffer (pH 5.6). The dose dependency of chymostatin was analyzed by the addition of various doses of chymostatin to aliquots of CPW, CPY, and the cell extracts of T1-PPCA and T1-PPCA(R344I) cell lines, and then, the mixtures were incubated for 30 min at 25 °C before the enzyme assays.

Protein Structures. The X-ray crystal structures obtained from the Research Collaboratory for Structural Bioinformatics Protein Data Bank,[29] including those of hCathA (PDB code: 1IVY),[13] CPW (PDB code: 1BCS),[17] and CPY (PDB code: 1YSC),[10] were used in this study. 1IVY has a symmetric dimeric precursor structure but was used to construct the monomeric form of hCathA in the following calculations. 1BCS is a cocrystal of CPW with chymostatin and arginine (Arg426), which was used to mimic the P1′ residue of the original substrate and was added for the stabilization of crystallization. Arg426 was removed in this study.

Three-dimensional structural similarity was obtained as the root-mean-squared deviation (RMSD) value by superimposition of the corresponding C_α atoms matched in the homology alignment.

Modeling of the Chymostatin-Carboxypeptidase Complex. The chymostatin−carboxypeptidase complex structural models were constructed on the basis of the X-ray crystal coordinates of the chymostatin−CPW complex (1BCS) by superimposing the crystal structures of the proteins and placing chymostatin in the corresponding position. The original 1BCS coordinates could be used because the RMSD value of each residue in the superimposed active sites was adequately low (discussed later). The maturation subdomain (Ala254-Pro302) of the hCathA precursor was removed for modeling of its active mature form.[13] It has been reported that peptidyl aldehyde inhibitors such as chymostatin form tetrahedral hemiacetal adducts with serine protease.[30−32] Active serine residues (hCathA, Ser150; CPW, Ser146; CPY, Ser146) are considered to bind to chymostatin via a covalent bond,[33−35] as shown in Figure 1b. This active Ser residue comprising the catalytic triad (charge relay system) with Asp and His residues is assumed to take on a dissociation state on complex formation (Figure 1b). The intermediate also has two optical isomers (*R* and *S*) because of the presence of an asymmetric carbon atom.

Water molecules inside the binding site were not taken into account in the present complex models because they were not observed at positions common in the three crystal structures. In the following calculations, the continuum solvent model was used instead of placing explicit water molecules.

Refinement of Chymostatin−Carboxypeptidase Complex Structures. For the refinement of the chymostatin−enzyme complex models, three-dimensional (3D) structural optimization was carried out with the MMFF94 force field[36] in Sybyl 6.9.[37] After 100 minimization cycles by the Powell method,[38] the structure was optimized by the conjugated gradient method[39] until the gradient value of each atom was below 0.1 kcal/mol/Å. After optimization, a short-time MD calculation (MMFF94, 300 K, 0.1 ps) was performed for annealing ill atomic contacts. Final energy minimization starting from the structure after MD was carried out until the gradient value was below 0.05 kcal/mol/Å. In the aforementioned procedures, the distance-dependent dielectric constant ($\epsilon = 4r$) was used for estimation of the electrostatic energy. The side chains of Arg and Lys were protonated and those of Asp and Glu were deprotonated in their charge states. The energy cutoff distance for electrostatic and nonbonded energies was taken as 8.0 Å, and the residues 8 Å away from chymostatin were fixed during optimization.

In addition to the three complex structures, the complex structure of a mutated hCathA(R344I) with chymostatin was constructed by means of the same procedures. The mutated hCathA contained Ile344 instead of Arg344 in the wild-type hCathA.

To evaluate the interaction energy between chymostatin and enzymes, the amino acid residues within 6 Å from the chymostatin molecule in the above complex structures ("full structure model") were extracted ("active-site model"). The extracted residues were terminally blocked with CH_3-CO- or $-NH-CH_3$, if necessary.

Molecular Orbital Calculation. The semiempirical molecular orbital method was applied at the AM1[40] level with the LocalSCF method[24] and the LocalSCF 2003 program.[41] Single-point calculations were carried out to estimate the interaction energy between chymostatin and each protein in the full structure and active-site models. The conductor-like screening model (COSMO)[42−44] was adopted to take into account the dielectric environment effect inside a protein. The initial localized molecular orbitals (LMOs) involved the Lewis core plus four chemical bonds around it. The threshold for derivatives for the expanding of LMOs and the maximum allowed nonorthogonality of orbitals were set to as 0.04 and 0.001, respectively.

Interaction Energy Evaluation. The binding energy is defined by eq 1.

$$\Delta E_{MO} = E(\text{complex}) - [E(\text{protein}) + E(\text{chymostatin})] \quad (1)$$

where the energetic terms in eq 1 were estimated with LocalSCF/AM1.

To reproduce the environment inside a protein effectively, the COSMO option was specified with the dielectric constant

values of $\epsilon = 4$ and 20 in addition to 1 (in a vacuum). The electrostatic interaction energy depends on the dielectric constant ϵ of a surrounding media. The dielectric constant ϵ inside a protein has been considered to be around 4.[45] However, the dielectric environment of a protein surrounded by water molecules is very inhomogeneous.[46] The effective dielectric constant ϵ^{eff} has been introduced to reproduce the electrostatic interaction of proteins effectively in the inhomogeneous environment. Using an ϵ^{eff} value between 4 and 20 was suggested by the Poisson−Boltzmann equation[47,48] and the protein dipoles Langevin dipoles[49] method. An ϵ^{eff} value between 1 and 40 was used in the self-consistent reaction field (SCRF)[50] MO calculations of proteins.[51,52] The value of ϵ^{eff} was taken as 1∼5 in the MM calculations of polypeptides.[53,54] Taking into account the aforementioned suggestions, we used $\epsilon^{eff} = 1$ (vacuum), 4, and 20 in the COSMO-MO calculations and compared these results carefully. The energy obtained by a SCRF model such as COSMO contains the solvation free energy partially at least. Also, the water-accessible surface area (*ASA*)[55−57] has been often utilized as a simple and quantitative parameter for change of the solvation free energy.[58] In this work, the solvation effect (solvation free energy) was quantitatively evaluated with the SCRF-MO calculation and the *ASA* parameter. The *ASA* value was calculated with a water probe radius of 1.4 Å and Bondi's van der Waals atomic radii[59] for each element. ΔASA was defined similarly to ΔE_{MO} in eq 1.

$$\Delta ASA = ASA(\text{complex}) - [ASA(\text{protein}) + ASA(\text{chymostatin})] \quad (2)$$

ΔASA in eq 2 expresses the surface area that disappeared on complex formation and is considered to be approximately proportional to the free energy change due to (de)hydration.

Energy Contribution from Amino Acid Residues. To clarify the interaction energy contribution from each amino acid residue around the binding site, electrostatic (E_{ele}) and van der Waals (E_{vdw}) interaction energies between each residue and chymostatin were calculated according to the Coulomb and Lenard-Jones equations, respectively. The atomic net charge was determined from the results of the LocalSCF/AM1 calculation, and the Lenard-Jones parameter values were taken from Amber91/STUB[60] (for H, C, N, O, and S). In addition to the E_{ele} and E_{vdw} terms, the contribution of ΔASA from each amino acid residue was calculated.

RESULTS

Similarity among hCathA, CPW, and CPY. Figure 2a shows the monomeric structural models of hCathA, CPW, and CPY determined on the basis of the X-ray crystal structures (PDB data). To construct the enzymatically active mature hCathA model, the sequence of the maturation subdomain (Ala254-Pro302) specific for the hCathA precursor was deleted manually from the X-ray coordinate data. The superimposition of them demonstrated the conformation of the backbone, and the side chains of the amino acid residues in the active sites of the constructed hCathA model, including the Ser-Asp-His catalytic triad and oxyanion hole, did not significantly change as compared with those of CPW and CPY (Figure 2b).

Table 1 shows the amino acid sequence homology and 3D similarity among the three proteins. The homology among the three proteins is above 30%, there being relatively high amino acid sequence similarity. The RMSD values as the parameter for 3D similarity obtained for the whole molecules were somewhat large, but those for the conserved amino acid residues in the catalytic triad and the oxyanion hole were lower than 0.35 Å among the three proteins (data not shown).

To predict the interaction of chymostatin with the active sites of hCathA and CPY, docking models of the chymostatin−enzyme complex were constructed on the basis of the crystallographic coordinates of the chymostatin−arginine complex with CPW.[17] Figure 3 summarizes the amino acid residues in the active sites (S1′ and S1−S4 subsites) of the enzymes possibly interacting with arginine at the P1′ position and the chymostatin molecule (P1−P4 residues). The common residues were predicted to be highly conserved in hCathA (Gly57, Cys60, Tyr151, Leu180, Cys334, and Asn339; Figure 3a), CPW (Gly53, Cys56, Tyr147, Leu178, Cys303, and Asn306; Figure 3b), and CPY (Gly53, Cys56, Tyr147, Leu178, Cys298, and Asn303; Figure 3c), suggesting that the inhibitor could interact with hCathA and CPY in a manner similar to that with CPW. However, there were still differences in amino acid residues among the enzymes (hCathA, Asp187, Phe336, and Arg344; CPW, Phe215, Ile216, Asp223, and Asp303b; CPY, Asn241, Phe300, and Trp312).

Interaction Energy of Chymostatin with hCathA, hCathA(R344I), CPW, and CPY. Our previous work demonstrated that different inhibitory effects of chymostatin on the wild-type hCathA, CPW, and CPY exist.[18] To explain the relative activity strength, the relative binding energies ($\Delta\Delta E_{MO}$) were calculated with LocalSCF/AM1 in this study, although the absolute value of the binding free energy change is difficult to determine by means of molecular calculations. As shown in Table 2, the calculated $\Delta\Delta E_{MO}$ values at $\epsilon = 4$ and 20 were in good agreement with the order of the observed activity values in Table 3. However, the electrostatic interaction energy was overestimated in the case of $\epsilon = 1$. The effective dielectric constant, ϵ, inside the binding site of a protein has been suggested to be between 4 and 20.[46−48]

As the absolute configuration of the tetrahedral intermediate indicates two possible isomers, *R* and *S*, we also calculated the relative interaction energy for both isomers. As shown in Table 2, the interaction energies of the *R* isomer at $\epsilon = 4$ and 20 were nearly equal to or lower than the corresponding ones of the *S* isomer, respectively. In the *R* isomer, the hemiacetal oxygen atom of chymostatin is accommodated in the oxyanion hole and undergoes hydrogen-bonding or electrostatic interaction with Gly residues (hCathA, Gly57; CPW, Gly53; CPY, Gly53) and Tyr residues (hCathA, Tyr151; CPW, Tyr147; CPY, Tyr147), as shown in Figure 3. In the *S* isomer, the oxygen atom faces His residues (hCathA, His429; CPW, His397; CPY, His397) and is not stabilized through interaction with any residues in the oxyanion hole. This suggests that the *R* isomer might be a more stable intermediate form than the *S* isomer.

Table 4 shows the results obtained for the active-site models, from which the interactions between chymostatin and its surrounding residues within 6 Å from the chymostatin were extracted, and only the *R* isomer was considered in the calculation. The $\Delta\Delta E_{MO}$ values in Table 4 were very similar to the corresponding ones in Table 2, indicating that

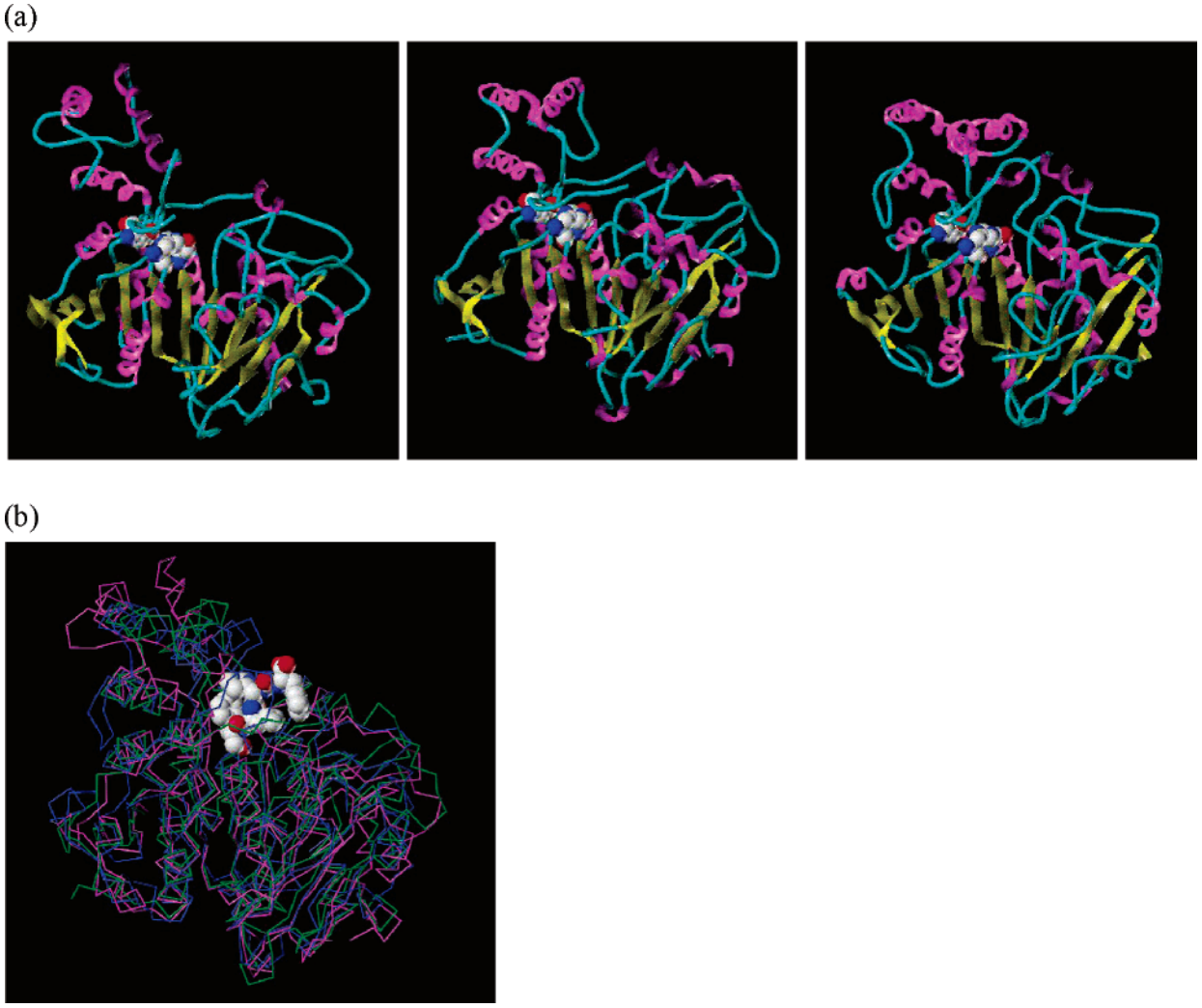

Figure 2. (a) Three-dimensional monomeric structures of hCathA (left), CPW (middle), and CPY (right) based on the X-ray crystal coordinates of each protein. The α helix and *β* sheet are colored in purple and yellow, respectively. Ser, Asp, and His residues in the catalytic triad are shown with the fill spacing model. (b) Three-dimensional superimposition among the chymostatin-complex models of hCathA (purple), CPW (green), and CPY (blue). Chymostatin is shown with the fill spacing model.

Table 1. Homology (%) and RMSD (Å) Values among Three Proteins

homology (%) RMSD (Å)	hCathA[a]	CPW	CPY
hCathA[a]	100	33.5	32.9
	0	6.8	6.5
CPW	33.5	100	30.1
	6.8	0	3.2
CPY	32.9	30.1	100
	6.5	3.2	0

[a] hCtah A contains the maturation subdomain.

several different amino acid residues around chymostatin among the three proteins determine the differences in their interaction energies.

Energy Contribution from the Amino Acid Residues around the Active Sites of Serine Carboxypeptidases. To determine the interaction energy contribution from the amino acid residues around a binding site, the interaction energies in the active-site models were further decomposed into the energies between each amino acid residue and chymostatin. Figures 4−6 show the ΔE_{ele}, ΔE_{vdw}, and ΔASA values for the wild-type hCathA (Figure 4), CPW (Figure 5), and CPY (Figure 6) obtained by the methods described above. These values in the catalytic triad and oxyanion hole were significantly negative for all three enzymes, suggesting their relatively stable interaction with chymostatin. However, these values were positive for a few residues around the binding site specific for each protein: Asp187 and Arg344 in the wild-type hCathA; Phe215, Ile216, and Asp223 in CPW; and Asn241 and Trp312 in CPY (Figure 3). Therefore, these specific residues possibly determine the selectivity of chymostatin as to the three enzymes. All of these specific residues were located in the S1 and S3 subsites, while most of the common residues among the three proteins were located in the S2 and S4 subsites.

As shown in Figures 4−6, analysis of the electrostatic interaction energy contribution from the specific residues in each protein predicted the following interactions: (Figure 4) in the wild-type hCathA, electrostatic repulsion between the cyclic arginine residue (guanidine moiety) in the P3 residue of chymostatin and the Arg344 residue in addition to significant attraction between the P3 residue and the Asp187 residue, (Figure 5) in CPW, attraction between the P3 moiety and the side chain of Asp223 as well as the peptide oxygen atoms of Phe215 and Ile216 residues, and (Figure

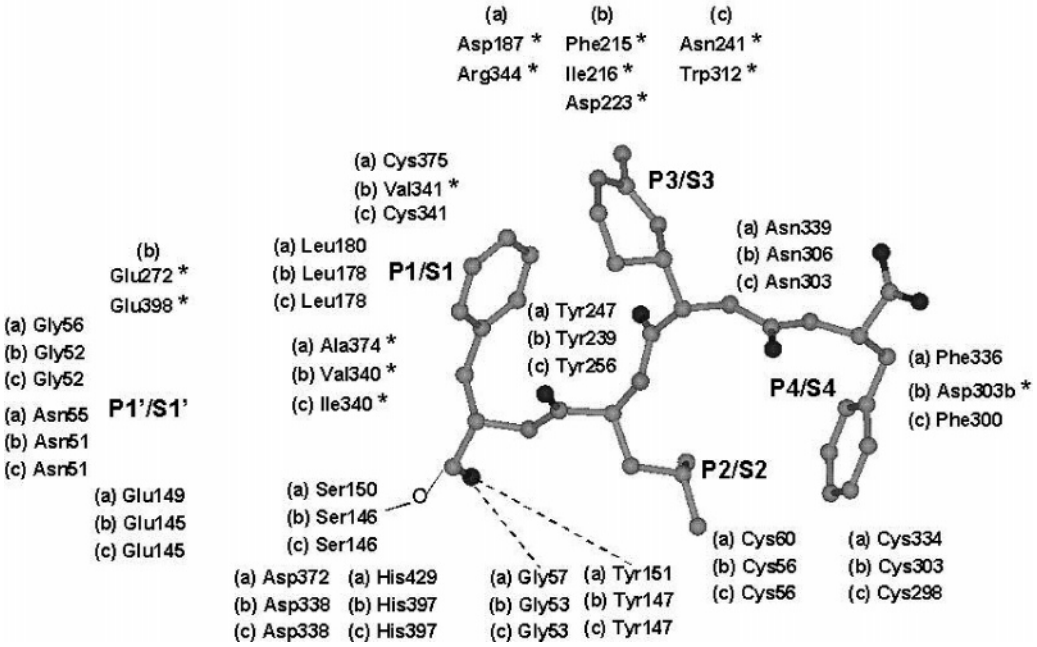

Figure 3. Comparison of amino acid residues around the binding site for chymostatin among (a) hCathA, (b) CPW, and (c) CPY. The residues marked by an asterisk are specific for each protein.

Table 2. Relative Binding Energy ($\Delta\Delta E_{MO}$) of Chymostatin with hCathA, CPW, and CPY in the Full Structure Model

		$\Delta\Delta E_{MO}$[a] (kcal/mol) dielectric constant (ϵ)		
	configuration	1	4	20
hCathA (wild)	*R*	8.1	−8.2	−14.9
		(−23.1)[b]	(15.8)[b]	(33.7)[b]
	S	4.0	−13.4	−21.2
		(−19.3)[b]	(16.9)[b]	(33.1)[b]
hCathA (R344I)	*R*	2.6	−17.1	−24.1
		(−28.5)[b]	(6.9)[b]	(24.5)[b]
	S	−2.4	−23.1	−34.1
		(−25.6)[b]	(7.2)[b]	(23.2)[b]
CPW	*R*	−11.7	−27.3	−31.7
		(−42.9)[b]	(−3.3)[b]	(16.9)[b]
	S	−13.4	−29.0	−33.9
		(−36.6)[b]	(1.3)[b]	(20.5)[b]
CPY	*R*	0	0	0
		(−31.1)[b]	(24.0)[b]	(48.6)[b]
	S	0	0	0
		(−23.3)[b]	(30.3)[b]	(54.4)[b]

[a] $\Delta\Delta E_{MO}[X]$ is defined by $\Delta E_{MO}[X] - \Delta E_{MO}[CPY(X)]$ ($X = R$ and *S* configurations). [b] The values in parentheses are the ΔE_{MO} values (binding energies).

Table 3. Inhibitory Activity of Chymostatin at pH 5.6

	IC_{50} (μM)	K_i (μM)	ΔG^{exp}[a] (kcal/mol)
hCathA (wild)	189.0 ± 28.6	59.2	−5.80
hCathA (R344I)	74.0 ± 1.9	5.7	−7.20
CPW	128 ± 28	37.8	−6.70
CPY	>200	N. A.[b]	N. A.[b]

[a] $\Delta G^{exp} = RT \ln K_i$ (300 K). [b] N. A. indicates not assayed.

6) in CPY, the absence of a negatively charged amino acid residue such as Asp223 in hCathA and Asp187 in CPW around the positively charged P3 moiety, although relatively weak attraction was revealed between the side chain of Asn241 and the P3 moiety.

As for the van der Waals interaction energy contribution, significant stabilization of the P1 (phenyl moiety) and P3 residues of chymostatin by the Phe215 and Ile216 residues in CPW (Figure 5), and by the Trp312 residue in CPY (Figure 6), was predicted. However, no specific residues with a large ΔE_{vdw} were observed for hCathA (Figure 4), as observed for CPW.

Table 4. Relative Binding Energy ($\Delta\Delta E_{MO}$) of Chymostatin with hCathA, CPW, and CPY in the Active-Site Model

		$\Delta\Delta E_{MO}$[a] (kcal/mol) dielectric constant (ϵ)		
	configuration	1	4	20
hCathA (wild)	*R*	7.8	−6.2	−12.6
		(−13.1)[b]	(19.2)[b]	(33.4)[b]
hCathA (R344I)	*R*	1.9	−14.8	−21.3
		(−19.0)[b]	(11.1)[b]	(24.7)[b]
CPW	*R*	−13.9	−24.4	−28.0
		(−34.8)[b]	(1.4)[b]	(18.1)[b]
CPY	*R*	0	0	0
		(−20.9)[b]	(25.9)[b]	(46.0)[b]

[a] $\Delta\Delta E_{MO}[X]$ is defined by $\Delta E_{MO}[X] - \Delta E_{MO}[CPY(X)]$ ($X = R$ configuration). [b] The values in parentheses are the ΔE_{MO} values (binding energies).

The amino acid residues contributing to the total ΔASA were similar to those contributing to ΔE_{vdw} among the three proteins.

As the most remarkable difference in interaction energy with chymostatin was predicted to be the electrostatic repulsion between the cyclic arginine residue (guanidine moiety) in the P3 residue of chymostatin and the Arg344 residue in the wild-type hCathA, we examined the effect of the amino acid substitution of Arg344 to Ile in hCathA on the inhibitory activity of chymostatin. Gene expression of the mutated hCathA(R344I) cDNA in a fibroblastic cell line derived from a galactosialidosis patient resulted in normal protein maturation and significant expression of carboxypeptidase activity at different pH's (Kadota et al., submitted), and then, the inhibitory activity of chymostatin toward the mutant hCathA(R344I) was compared to that of the wild-type hCathA, CPW, and CPY. As shown in Table 3, the

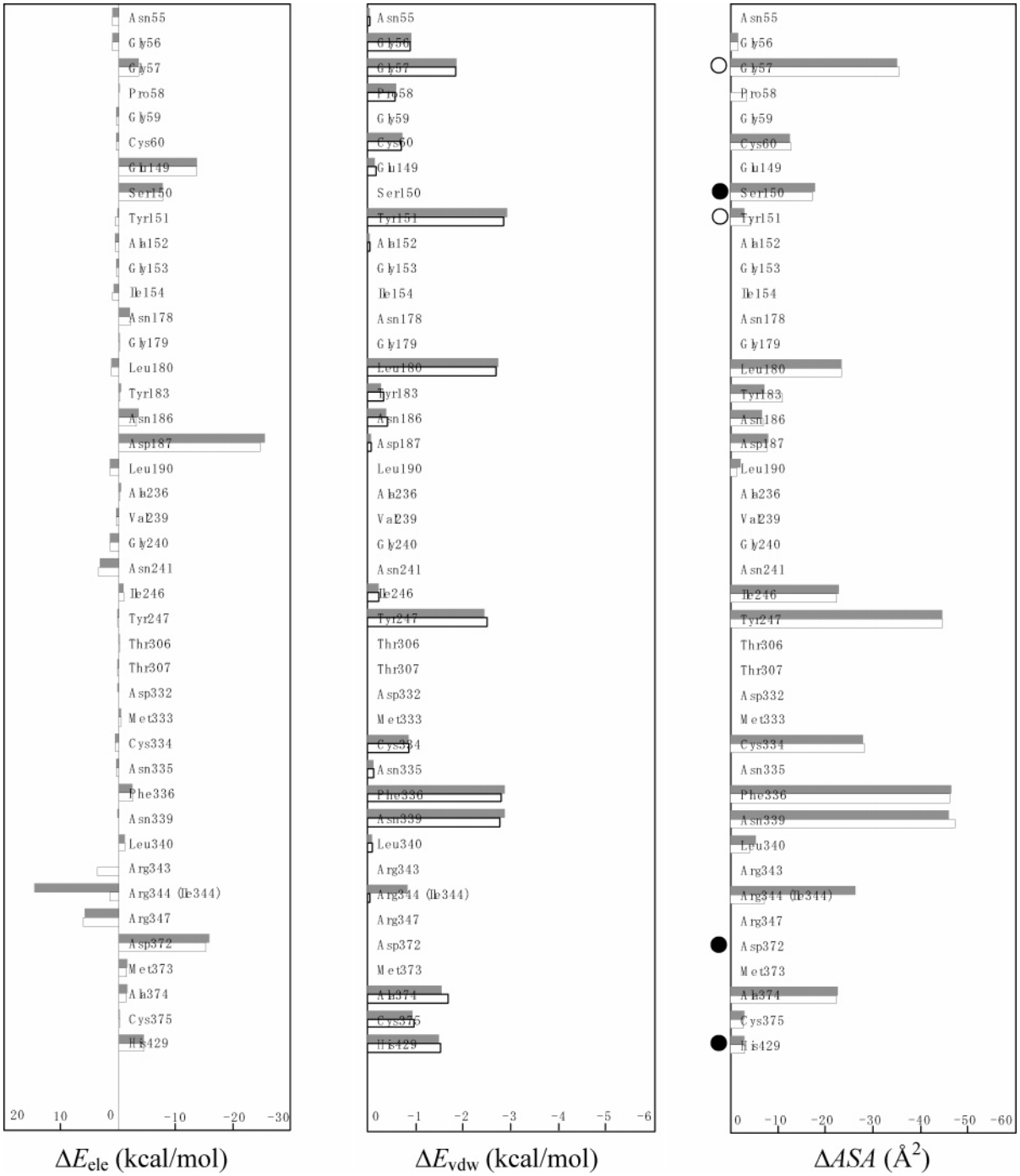

Figure 4. Contribution of the ΔE_{ele}, ΔE_{vdw}, and ΔASA values from each amino acid around the binding site for chymostatin for hCathA (white bars indicate the values for hCathA-R344I). The residues located in the catalytic triad and oxyanion hole are marked with ● and ○, respectively.

sensitivity of hCathA(R344I) to the inhibitor was revealed to be more increased than that of the wild-type hCathA and CPW. These results strongly suggest that the electrostatic repulsion between the P3 moiety of chymostatin and the Arg344 residue was abolished by the mutation causing the amino acid substitution (Arg344 to Ile) and the change in net charge of the residue from +1 to 0.

Tables 2 and 4 also demonstrate the correlation between the increase in the sensitivity of hCathA(R344I) to chymostain and the decrease in the calculated $\Delta\Delta E_{MO}$ value both in the full structure and in the active-site model. Accordingly, the hCathA(R344I)−chymostatin complex was considered to be more stabilized because of this amino acid substitution, judging from the decrease in the total interaction energy.

DISCUSSION

In this study, we constructed structural models of hCathA and homologous serine carboxypeptidases (CPW and CPY) on the basis of their X-ray crystal coordinates. hCathA is synthesized as a precursor dimer that comprises a core domain (residues 1−182 and 303−452) and a cap domain (residues 183−302).[5,13] The latter domain further consists of a helical subdomain (residues 183−253) and a maturation subdomain (residues 254−302). The latter subdomain in-

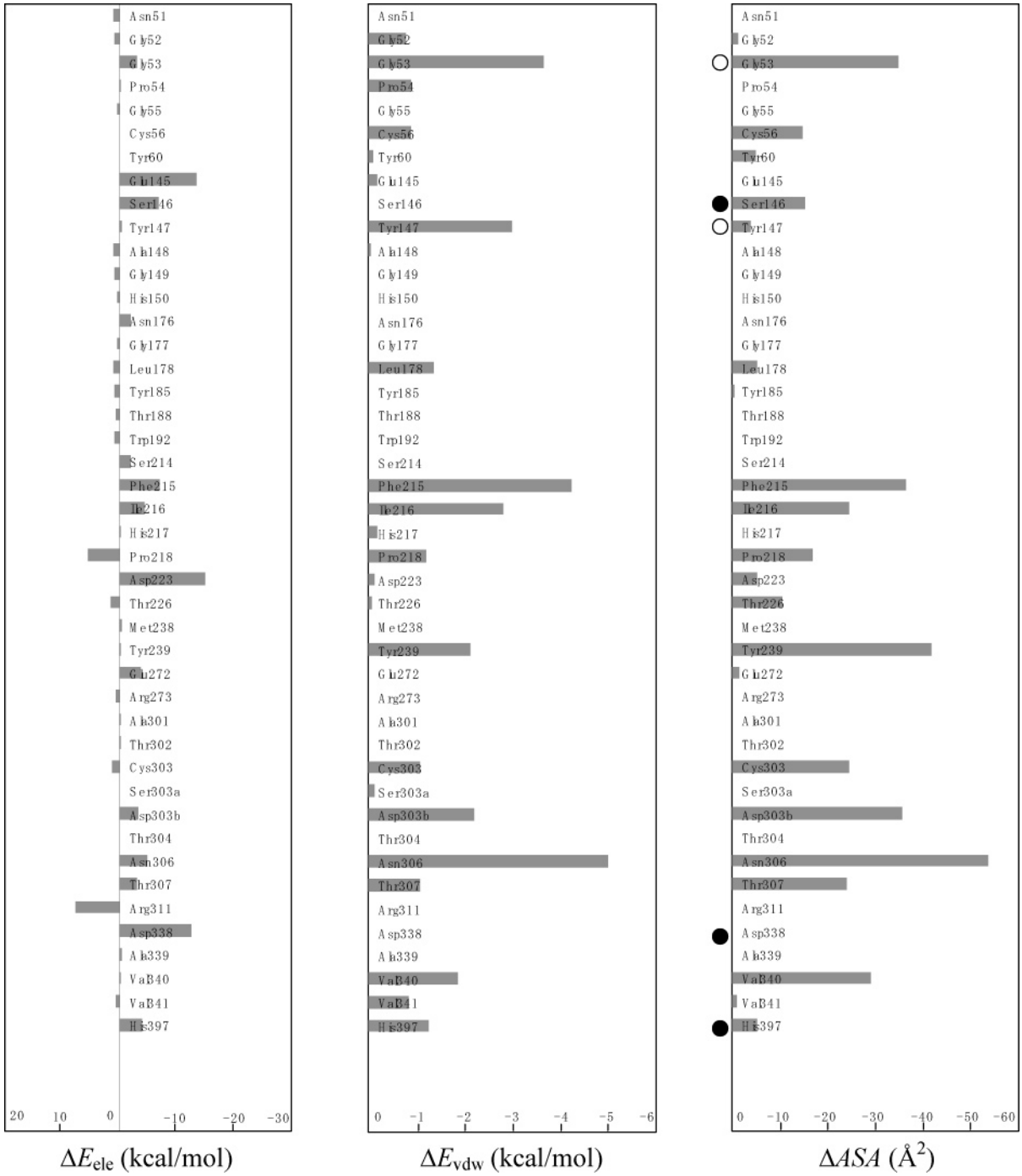

Figure 5. Contribution of the ΔE_{ele}, ΔE_{vdw}, and ΔASA values from each amino acid around the binding site for chymostatin for CPW. The residues located in the catalytic triad and oxyanion hole are marked with ● and ○, respectively.

cludes a blocking peptide (residues 272−277) and an excision peptide (residues 285−298), which is not conserved in CPW and CPY. The excision peptide is further cleaved off from the precursor protein for the expression of catalytic activity in vivo.[2,5] Therefore, the hCathA monomer model, as an enzymatically active mature form, was built by removing the amino acid sequence corresponding to the total maturation subdomain (residues 254−302). As a result, the conformations of the conserved active sites including the Ser-Asp-His catalytic triad and oxyanion hole were predicted to be very similar among the present models.

As previously reported, chymostatin, one of the potent inhibitors of chymotrypsin,[16] also exhibited an inhibitory effect on CPW and hCathA, while it had less effect on CPY.[18] To characterize the differences in sensitivity to chymostatin among the homologous serine carboxypeptidases, we also built chymostatin−enzyme complex models based on the crystallographic structure of the chymostatin−arginine−CPW complex.[17] It was demonstrated in that report that chymostatin formed a covalent adduct with the active Ser146 residue of CPW and that all four residues (P1−P4) of the inhibitor fitted well to the corresponding S1 through S4 subsites in the active-site cleft.

The present molecular calculation study performed to compare the binding energy for chymostatin and the homologous serine carboxypeptidases in the complex models predicted a conserved interaction between the inhibitor moieties and the common amino acid residues in the active-

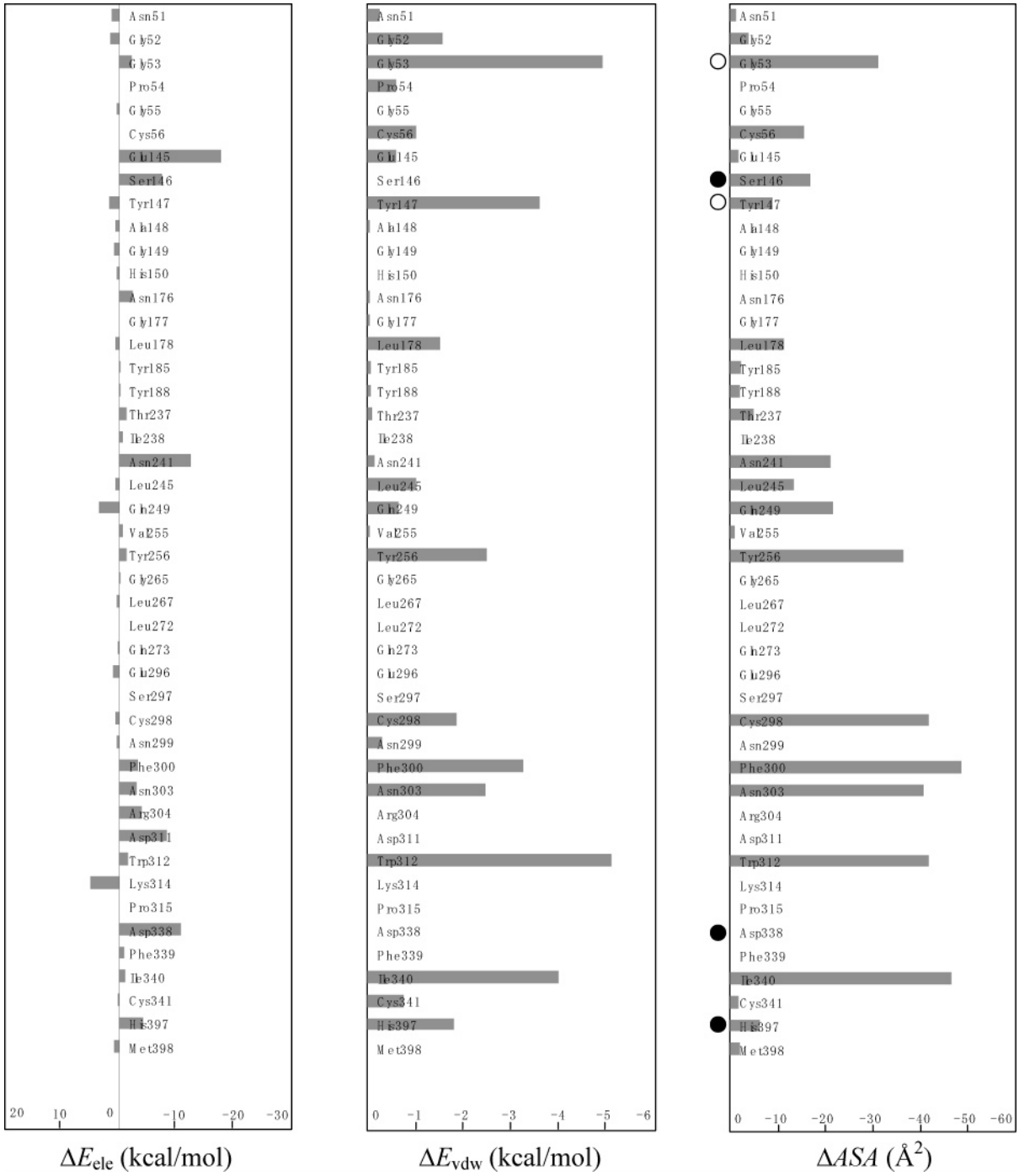

Figure 6. Contribution of the ΔE_{ele}, ΔE_{vdw}, and ΔASA values from each amino acid around the binding site for chymostatin for CPY. The residues located in the catalytic triad and oxyanion hole are marked with ● and ○, respectively.

site cleft including the catalytic triad and oxyanion hole, which are necessary for expression of their catalytic activities. This work also suggested that the differences in inhibitory activity of chymostatin toward the three homologous enzymes can be explained by the differences in interaction energy between the inhibitor as a ligand and the enzymes as receptors. The sensitivity of each enzyme to chymostatin was considered to be governed by a few different amino acid residues located in their S1 and S3 subsites. The Arg344 residue in the active site of the wild-type hCathA was predicted to exhibit electrostatic repulsion from the P3 cyclic arginine residue (guanidine moiety) of chymostatin in this binding energy calculation. An increased IC_{50} value of chymostatin compared to the wild-type hCathA was observed at pH 4.0 (data not shown), compared with that in the case of pH 5.6. This finding suggested that such charge−charge repulsion also became strong because the dissociative ratio of the Arg344 residue and P3 cyclic arginine side chains increased at the more acidic pH of 4.0. Interestingly, genetic conversion of the Arg344 residue to Ile, Met, or Val (data shown for Ile only) caused a significant increase in the sensitivity to chymostatin, strongly supporting that the hypothesis is correct. We had previously demonstrated that the carboxyl terminus of endothelin-1, one of the endogenous peptidic substrates, was degraded by CathA and that the enzyme activity was deficient in patients with galactosialidosis caused by mutations of the PPCA gene.[3,8] Endothelin-1 retains the carboxyl terminal amino acid sequence, -Leu-

Asp-Ile-Ile-Trp, corresponding to the P4−P3−P2−P1−P1′ positions, which is essential for expression of its biological activities. Taking into account the presence of the Arg344 residue in the S3 subsite of hCathA, it may be reasonable that endothelin-1 with an Asp residue at the P3 position could be a preferred substrate for hCathA necessary for expressing the catalytic activity. As the pathophysiological roles of the hCathA activity in vivo have not been fully elucidated, it is desirable to develop a specific inhibitor for the enzyme as a tool. The results obtained in this study will enable us to design a more selective and potent inhibitor of hCathA by means of molecular calculations. The calculations here can provide the correct orders in the experimental potency of binding: CPW > hCathA(wild-type) > CPY and hCathA-(R344I) > hCathA(wild-type). However, the experimental order between hCathA(R344I) and CPW could not be correctly reproduced by the calculations. To predict the experimental affinities of hCathA(R344I) and CPW quantitatively by the calculations, it probably requires more careful and sophisticated computational procedures. Further efforts for this problem are in progress to obtain more reliable binding energies.

Finally, determination of the interaction energy between the inhibitor and enzymes could be utilized to evaluate the energetically favorable and unfavorable structural states in both cases, which is expected to be applicable to the development of a novel probe and drugs specific for target proteins.

ACKNOWLEDGMENT

We wish to thank Dr. S. Aikawa and M. S. F. Matsuzawa (Celestar Lexico-Sciences, Inc., Chiba, Japan) for providing the structural data and technical assistance. This work was supported by the Technology of Japan Science and Technology Corporation (JST-CREST) and the 21st Century COE Program, Human Nutritional Science on Stress Control, Tokushima, Japan.

REFERENCES AND NOTES

(1) Jackman, H. L.; Tan, F. L.; Tamei, H.; Beurling-Harbury, C.; Li, X. Y.; Skidgel, R. A.; Erdos, E. G. A peptidase in human platelets that deamidates tachykinins. Probable identity with the lysosomal "protective protein". *J. Biol. Chem.* **1990**, *265*, 11265−11272.

(2) Itoh, K.; Takiyama, N.; Kase, R.; Kondoh, K.; Sano, A.; Oshima, A.; Sakuraba, H.; Suzuki, Y. Purification and characterization of human lysosomal protective protein expressed in stably transformed Chinese hamster ovary cells. *J. Biol. Chem.* **1993**, *268*, 1180−1186.

(3) Itoh, K.; Kase, R.; Shimmoto, M.; Satake, A.; Sakuraba, H.; Suzuki, Y. Protective protein as an endogenous endothelin degradation enzyme in human tissues. *J. Biol. Chem.* **1995**, *270*, 515−518.

(4) d'Azzo, A.; Andria, G.; Strisciuglio, P.; Galjaard, H. In *The Metabolic and Molecular Bases of Inherited Disease*, 8th ed.; Scriver, C. R., Beaudet, A. L., Sly, W. S., Valle, D., Eds.; McGraw-Hill: New York, 2000; pp 3811−3826.

(5) Galjart, N. J.; Gillemans, N.; Harris, A.; van der Horst, G. T.; Verheijen, F. W.; Galjaard, H.; d'Azzo, A. Expression of cDNA encoding the human "protective protein" associated with lysosomal beta-galactosidase and neuraminidase: Homology to yeast proteases. *Cell* **1998**, *54*, 755−764.

(6) Pshezhetsky, A. V.; Elsliger, M. A.; Vinogradova, M. V.; Potier, M. Human lysosomal beta-galactosidase-cathepsin A complex: Definition of the beta-galactosidase-binding interface on cathepsin A. *Biochemistry* **1995**, *34*, 2431−2440.

(7) Shimmoto, M.; Fukuhara, Y.; Itoh, K.; Oshima, A.; Sakuraba, H.; Suzuki, Y. Protective protein gene mutations in galactosialidosis. *J. Clin. Invest.* **1993**, *91*, 2393−2398.

(8) Itoh, K.; Oyanagi, K.; Takahashi, H.; Sato, T.; Hashizume, Y.; Shimmoto, M.; Sakuraba, H. Endothelin-1 in the brain of patients with galactosialidosis: Its abnormal increase and distribution pattern. *Ann. Neurol.* **2000**, *47*, 122−126.

(9) Reminigton, S. J.; Breddam, K. Carboxypeptidases C and D. *Methods Enzymol.* **1994**, *244*, 231−248.

(10) Endrizzi, J. A.; Breddam, K.; Remington, S. J. 2.8-Å structure of yeast serine carboxypeptidase. *Biochemistry* **1994**, *33*, 11106−11120.

(11) Bullock, T. L.; Branchaud, B.; Remington, S. J. Structure of the complex of L-benzylsuccinate with wheat serine carboxypeptidase II at 2.0-Å resolution. *Biochemistry* **1994**, *33*, 11127−11134.

(12) Elsliger, M. A.; Pshezhetsky, A. V.; Vinogradova, M. V.; Svedas, V. K.; Potier, M. Comparative modeling of substrate binding in the S1′ subsite of serine carboxypeptidases from yeast, wheat, and human. *Biochemistry* **1996**, *35*, 14899−14909.

(13) Rudenko, G.; Bonten, E.; d'Azzo, A.; Hol, W. G. Three-dimensional structure of the human 'protective protein': Structure of the precursor form suggests a complex activation mechanism. *Structure* **1995**, *3*, 1249−1259.

(14) Ollis, D. L.; Cheah, E.; Cygler, M.; Dijkstra, B.; Frolow, F.; Franken, S. M.; Harel, M.; Remington, S. J.; Silman, I.; Schrag, J.; Sussman, J. L.; Verschueren, K. H. G.; Goldman, A. The alpha/beta hydrolase fold. *Protein Eng.* **1992**, *5*, 197−211.

(15) Remington, S. J. Serine carboxypeptidases: A new and versatile family of enzymes. *Curr. Opin. Biotechnol.* **1993**, *4*, 462−468.

(16) Umezawa, H. Structures and activities of protease inhibitors of microbial origin. *Methods Enzymol.* **1976**, *45*, 678−695.

(17) Bullock, T. L.; Breddam, K.; Remington, S. J. Peptide aldehyde complexes with wheat serine carboxypeptidase II: Implications for the catalytic mechanism and substrate specificity. *J. Mol. Biol.* **1996**, *255*, 714−725.

(18) Satoh, Y.; Kadota, Y.; Oheda, Y.; Kuwahara, J.; Aikawa, S.; Matsuzawa, F.; Doi, H.; Aoyagi, T.; Sakuraba, H.; Itoh, K. Microbial serine carboxypeptidase inhibitors: Comparative analysis of actions on homologous enzymes derived from man, yeast and wheat. *J. Antibiot. (Tokyo)* **2004**, *57*, 316−325.

(19) Chandrasekhar, J.; Jorgensen, W. L. Energy profile for a nonconcerted S_N2 reaction in solution. *J. Am. Chem. Soc.* **1985**, *107*, 2974−2975.

(20) Huetz, P.; Kamarulzaman, E. E.; Wahab, H. A.; Mavri, J. Chemical reactivity as a tool to study carcinogenicity: Reaction between estradiol and estrone 3,4-quinoes ultimate carciogens and guanine. *J. Chem. Inf. Comput. Sci.* **2004**, *44*, 310−314.

(21) Warshel, A.; Levitt, M. Theoretical studies of enzymic reactions: Dielectric, electrostatic and steric stabilization of the carbonium ion in the reaction of lysozyme. *J. Mol. Biol.* **1976**, *103*, 227−249.

(22) Guimaraes, C. R.; Udier-Blagovic, M.; Jorgensen, W. L. Macrophomate synthase: QM/MM simulations address the Diels−Alder versus Michael−Aldol reaction mechanism. *J. Am. Chem. Soc.* **2005**, *127*, 3577−3588.

(23) Gogonea, V.; Westerhoff, L. M.; Merz, K. M., Jr. Quantum mechanical/quantum mechanical methods. I. A divide and conquer strategy for solving the Schrödinger equation for large molecular systems using a composite density functional-semiempirical Hamiltonian. *J. Chem. Phys.* **2000**, *113*, 5604−5613.

(24) Anikin, N. A.; Aisimov, V. M.; Buganeko, V. L.; Bobrikov, V. V.; Andreyev, A. M. LocalSCF method for semiempirical quantum-chemical calculation of ultralarge biomolecules. *J. Chem. Phys.* **2004**, *121*, 1266−1270.

(25) Kitaura, K.; Sawai, T.; Asada, T.; Nakano, T.; Uebayasi, M. Pair interaction molecular orbital method: An approximate computational method for molecular interactions. *Chem. Phys. Lett.* **1999**, *312*, 319−324.

(26) Fukuzawa, K.; Kitaura, K.; Uebayasi, M.; Nakata, K.; Kaminuma, T.; Nakano, T. Ab initio quantum mechanical study of the binding energies of human estrogen receptor alpha with its ligands: An application of fragment molecular orbital method. *Comput. Chem.* **2005**, *26*, 1−10.

(27) Fukuzawa, K.; Komeiji, Y.; Mochizuki, Y.; Kato, A.; Nakano, T.; Tanaka, S. Intra- and intermolecular interactions between cyclic-AMP receptor protein and DNA: Ab initio fragment molecular orbital study. *J. Comput. Chem.* **2006**, *27*, 948−960.

(28) Dixon, M. The determination of enzyme inhibitor constants. *Biochem. J.* **1953**, *55*, 70−71.

(29) The RCSB Protein Data Bank. http://www.rcsb.org/pdb/ (accessed Jul 2006).

(30) Kurinov, I. V.; Harrison, R. W. Two crystal structures of the leupeptin−trypsin complex. *Protein Sci.* **1996**, *5*, 752−758.

(31) Delbaere, L. T.; Brayer, G. D. Structure of product and inhibitor complexes of streptomyces griseus protease A at 1.8 Å resolution. *J. Mol. Biol.* **1980**, *144*, 43−88.

(32) Delbaere, L. T.; Brayer, G. D. The 1.8 Å structure of the complex between chymostatin and streptomyces griseus protease A. A model for serine protease catalytic tetrahedral intermediates. *J. Mol. Biol.* **1985**, *183*, 89−103.

(33) Neidhart, D.; Wei, Y.; Cassidy, C.; Lin, J.; Cleland, W. W.; Frey, P. A. Correlation of low-barrier hydrogen bonding and oxyanion binding in transition state analogue complexes of chymotrypsin. *Biochemistry* **2001**, *40*, 2439−2447.
(34) Pechenov, A.; Stefanova, M. E.; Nicholas, R. A.; Peddi, S.; Gutheil, W. G. Potential transition state analogue inhibitors for the penicillin-binding proteins. *Biochemistry* **2003**, *42*, 579−588.
(35) Bott, R. R.; Chan, G.; Domingo, B.; Ganshaw, G.; Hsia, C. Y.; Knapp, M.; Murray, C. J. Do enzymes change the nature of transition states? Mapping the transition state for general acid−base catalysis of a serine protease. *Biochemistry* **2003**, *4*, 10545−10553.
(36) Thomas, A. H. Maximally diagonal force constants in dependent angle-bending coordinates. 2. Implications for the design of empirical force fields. *J. Am. Chem. Soc.* **1990**, *112*, 4710−4723.
(37) *Sybyl6.9*; Tripos Inc.: St. Louis, Missouri. http://www.tripos.com (accessed Jul 2006).
(38) Powell, M. J. D. Restart procedures for the conjugate gradient method. *Math. Programming* **1977**, *12*, 241−254.
(39) Press, W. H.; Flannery, B. P.; Teukolsky, S. A.; Vetterling, W. T. In *Numerical Recipes in C; The Art of Scientific Computing*, 2nd ed.; Cambridge University Press: New York, 1988; p 301.
(40) Dewar, M. J. S.; Zoebisch, E. G.; Healy, E. F.; Stewart, J. J. P. Development and use of quantum mechcanical moleculr models. 76. AM1: A new general purpose quantum mechanical molecular model. *J. Am. Chem. Soc.* **1985**, *107*, 3902−3909.
(41) *LocalSCF 2003 Program*; Fujitsu Limited: Tokyo, Japan, 2003.
(42) Klamt, A.; Schuurmann, G. COSMO: A new approach to dielectric screening in solvents with explicit expressions for the screening energy and its gradient. *J. Chem. Soc., Perkin Trans.* **1993**, *2*, 799−805.
(43) Klamt, A.; Jonas, V. Refinement and parameterization of COSMO-RS. *J. Phys. Chem.* **1998**, *102*, 5074−5085.
(44) Klamt, A.; Eckert, F.; Hornig, M.; Beck, M. E.; Burger, T. Prediction of aqueous solubility of drugs and pesticides with COSMO-RS. *J. Comput. Chem.* **2002**, *33*, 275−281.
(45) Schultz, G. E.; Schirmer, R. H. *Principles of Protein Structure*; Springer-Verlag: New York, 1979.
(46) Warshel, A.; Papazyan, A. Electrostatic effects in macromolecules: Fundamental concepts and practical modeling. *Curr. Opin. Struct. Biol.* **1998**, *8*, 211−217.
(47) Antosiewicz, J.; McCammon, J. A.; Gilson, M. K. Prediction of pH-dependent properties of proteins. *J. Mol. Biol.* **1994**, *238*, 415−436.
(48) Antosiewicz, J.; McCammon, J. A. The determinants of pK_as in proteins. *Biochemistry* **1996**, *35*, 7819−7833.
(49) Sham, Y. Y.; Muegge, I.; Warshel, A. The effect of protein relaxation on charge−charge interactions and dielectric constants of protein. *Biophys. J.* **1998**, *74*, 1744−1753.
(50) Tapia, O.; Goscniski, O. Self-consistent reaction field theory of solvent effects. *Mol. Phys.* **1975**, *29*, 1653−1661.
(51) Siegbahn, P. E. M.; Blomberg, M. R. A.; Pavlov, M. A comparison of electron transfer in ribonucleotide reductase and the bacterial photosynthetic reaction center. *Chem. Phys. Lett.* **1998**, *292*, 421−430.
(52) Shokhen, M.; Albeck, A. Identification of protons position in acid−base enzyme catalyzed reactions: The hepatitis C viral NS3 protease. *Proteins* **2004**, *55*, 245−250.
(53) Momany, F. A.; McGuire, R. F.; Burgess, A. W.; Scheraga, H. A. Energy parameters in polypeptides. VII. Geometric parameters, partial atomic charges, nonbonded interactions, hydrogen bond interactions, and instrinsic torsional potentials for the naturally occurring amino acids. *J. Phys. Chem.* **1975**, *79*, 2361−2381.
(54) Brant, D. A. Conformational analysis of biopolymers: Conformational energy calculations. *Annu. Rev. Biophys. Bioeng.* **1972**, *1*, 369−408.
(55) Hermann, R. B. Theory of hydrophobic bonding. II. The correlation of hydrocarbon solubility in water with solvent cavity surface area. *J. Phys. Chem.* **1972**, *76*, 2754−2759.
(56) Chothia, C. Hydrophobic bonding and accessible surface area in proteins. *Nature (London)* **1974**, *248*, 338−339.
(57) Honig, B.; Sharp, K.; Yang, A.-S. Macroscopic models of aqueous solutions: Biological and chemical applications. *J. Phys. Chem.* **1993**, *97*, 1101−1109.
(58) Chuman, H.; Mori, A.; Tanaka, H.; Yamagami, C.; Fujita, T. Analyses of the partition coefficient, Log P, using ab initio MO parameter and accessible surface area of solute molecules. *J. Pharm. Sci.* **2004**, *93*, 2681−2697.
(59) Bondi, A. Van der Waals volumes and radii. *J. Phys. Chem.* **1964**, *68*, 441−451.
(60) Weiner, S. J.; Kollman, P. A.; Case, D. A.; Singh, U. C.; Ghio, C.; Alagona, G.; Profeta, S.; Weiner, P. A new force field for molecular mechanical simulation of nucleic acids and proteins. *J. Am. Chem. Soc.* **1984**, *106*, 765−784.

CI060093P